Dynamics of Fusion Pores Connecting Membranes of Different Tensions

Yuri A. Chizmadzhev,* Peter I. Kuzmin,* Dimetry A. Kumenko,* Joshua Zimmerberg,† and Fredric S. Cohen‡
*Frumkin Institute of Electrochemistry, Moscow, Russia; †Laboratory of Cellular and Molecular Biophysics, National Institutes of Child Health and Human Development, Bethesda, Maryland 20892 USA; and ‡Department of Molecular Biophysics and Physiology, Rush Medical College, Chicago, Illinois 60612 USA

ABSTRACT The energetics underlying the expansion of fusion pores connecting biological or lipid bilayer membranes is elucidated. The energetics necessary to deform membranes as the pore enlarges, in some combination with the action of the fusion proteins, must determine pore growth. The dynamics of pore growth is considered for the case of two homogeneous fusing membranes under different tensions. It is rigorously shown that pore growth can be quantitatively described by treating the pore as a quasiparticle that moves in a medium with a viscosity determined by that of the membranes. Motion is subject to tension, bending, and viscous forces. Pore dynamics and lipid flow through the pore were calculated using Lagrange's equations, with dissipation caused by intra- and intermonolayer friction. These calculations show that the energy barrier that restrains pore enlargement depends only on the sum of the tensions; a difference in tension between the fusing membranes is irrelevant. In contrast, lipid flux through the fusion pore depends on the tension difference but is independent of the sum. Thus pore growth is not affected by tension-driven lipid flux from one membrane to the other. The calculations of the present study explain how increases in tension through osmotic swelling of vesicles cause enlargement of pores between the vesicles and planar bilayer membranes. In a similar fashion, swelling of secretory granules after fusion in biological systems could promote pore enlargement during exocytosis. The calculations also show that pore expansion can be caused by pore lengthening; lengthening may be facilitated by fusion proteins.

INTRODUCTION

The growth of fusion pores is poorly understood. Fusion proteins play a major role in creating a pore, but their importance to pore expansion is unclear. Regardless of the specific mechanisms that are controlled by the proteins, the membranes that comprise the pore wall must deform as a pore grows. It is even possible that fusion proteins exert their effect on pore growth by regulating these deformations. Independent of the contribution of fusion proteins to pore expansion, the underlying physics of the membrane deformations must be a critically important aspect of the process. The work required to deform membranes depends strongly on membrane tensions, and therefore the tension of fusing membranes must affect the rate of pore growth. This is observed (Solsona et al., 1998; Markosyan et al., 1999). In general, the tensions of two membranes will be different, and after the membranes fuse the tensions will equilibrate to a common intermediate value. In cellular situations, tensions of plasma membranes can be substantial (Waugh and Bauserman, 1995). Membrane tensions of intracellular compartments may be larger than those of plasma membranes, and the membrane tensions of these compartments can be different: exocytotic granule membranes are thought to be under significantly more tension than plasma membranes (Monck et al., 1990; Solsona et al., 1998). Some secretory granules swell upon formation of a fusion pore (Zimmerberg et al., 1987; Curran and Brodwick, 1991; Marszalek et al., 1997) and may thereby create an additional and substantial tension. Moreover, postfusion convective flow of Golgi into endoplasmic reticulum membrane appears to be driven by tension differences (Sciaky et al., 1997). In model systems, the tensions and their differences can be even greater. For fusion of two planar membranes made from different lipids (Chernomordik et al., 1987), the tension differences will not change over time because each planar membrane tension is maintained by its Gibbs-Plateau border. To fuse liposomes to planar membranes, the liposomes are routinely swelled (Zimmerberg et al., 1980; Cohen et al., 1980) to increase their membrane tension. This promotes both fusion (Cohen and Niles, 1993) and pore expansion (Chernomordik et al., 1995; Chanturiya et al., 1997).

We previously derived equations that describe lipid flow through a fusion pore of any fixed size that connects two membranes of different tensions (Chizmadzhev et al., 1999). The current paper extends these equations to investigate the dynamics of pore growth. We considered pore growth as movement of the pore wall caused by two forces. The first are the tension and bending forces and the second are the viscous forces derived by standard membrane mechanics (Evans and Skalak, 1980). Fusion pore dynamics and lipid flux were both calculated using Lagrange's equations with dissipation (Goldstein, 1950). The dissipation was described as a shear friction within monolayers and a relative friction due to lipids moving past each other in different monolayers. Because an initial pore may form within a hemifusion diaphragm—a bilayer that continues to separate aqueous contents after the contacting monolayer leaflets have merged—we considered lipid flux through these pores and pore growth as well. Our equations are

Received for publication 1 September 1999 and in final form 8 January 2000.

Address reprint requests to Dr. Frederic S. Cohen, Department of Physiology, Rush Medical College, 1750 West Harrison St., Chicago, IL 60612-3864. Tel.: 312-942-6753; Fax: 312-942-8711; E-mail: fcohen@rush.edu.

0006-3495/00/05/2241/16 $2.00

clearly applicable to the fusion of pure lipid bilayers. They are also directly applicable to biological fusion pores once they have grown beyond their initial state because their walls should have characteristics typical of biological membranes. The results of our calculations show that pore widening can be promoted by pore lengthening. If the fusion proteins regulated pore length, they would be able to control the process of pore growth via that single parameter.

MODELING THE FUSION PORE

The geometry of the system

In general, as long as a pore's radius is much smaller than the size of the fusing objects, the two membranes can be considered planar and parallel to each other, connected by the fusion pore. We thus conceptualize a fusion pore as being of toroidal shape, connecting two parallel planar bilayers each of thickness $2h$, whose neutral surfaces (the interfaces between the two monolayers) are separated by $2H$ (Fig. 1 *A*). This geometry is exactly as described previously (Chizmadzhev et al., 1999), but in the present study we allow the pore radius to vary. As previously, H is kept constant. The system is cylindrically symmetrical about the z axis. The pore radius R is defined as the distance from the z axis, which passes through the center of the pore, to the junction between the toroidal and planar surfaces. The radius of the narrowest portion of the lumen of the pore is $r_p = R - (H + h)$. The radius of the fusing objects (e.g., a planar membrane or cell) is given by $R_m \gg R$. σ_1 and σ_2 designate the tensions of single monolayers in the upper (*1*) and lower (*2*) membranes (Fig. 1 *A*). The two bilayer tensions are different, $2\sigma_1 > 2\sigma_2$, and are kept constant at R_m. Cylindrical coordinates (r, z, θ) describe the geometry of the planar membranes (Fig. 1). For the toroidal portion, we use the specialized coordinates (θ, φ, ρ), where ρ takes on values within the interval $H + h > \rho > H - h$, the angle φ is confined to the interval $[-\pi/2, \pi/2]$ (Fig. 1 *A*), and the azimuthal angle θ lies in the interval $[0, 2\pi]$ (Fig. 1 *B*). H and h remain constant, but the pore radius (R or r_p) is time dependent.

Simplifying monolayers as two-dimensional surfaces

In deriving the equations, we treat the fused membranes as homogeneous lipid bilayers. We extend the results to biological membranes in the Discussion.

For a pore to expand, lipids must redistribute between the pore wall and planar membranes, and hence pore expansion and lipid movement are intimately associated. In this paper we derive equations for the rate of growth of a toroidal fusion pore when the tensions of the membranes, $2\sigma_1$ and $2\sigma_2$, are different. Because the tensions are different, lipid will flow from one membrane to the other (Chizmadzhev et al., 1999). For any given pore radius, the distribution of these lipid velocities within the membranes will quickly reach steady state. Thus, at any moment, the work performed by membrane tension in causing lipid flow and pore growth is equal to the dissipation of energy due to viscosity. Two types of viscosity are involved in lipid movement. The first originates from lipid-lipid and lipid-protein interactions within each monolayer. These shear deformations, described by a shear viscosity η_s, are present in both the planar membrane and toroidal pore when lipid moves. The second viscosity arises from friction between lipid monolayers as they move past each other, described by a relative viscosity, η_r. The viscous friction between a monolayer and the bathing water is negligibly small (Chizmadzhev et al., 1999).

Lipid flow within a curved toroidal pore is complicated by the fact that the areas available to the lipid headgroups and acyl chains within a monolayer are different. Within the

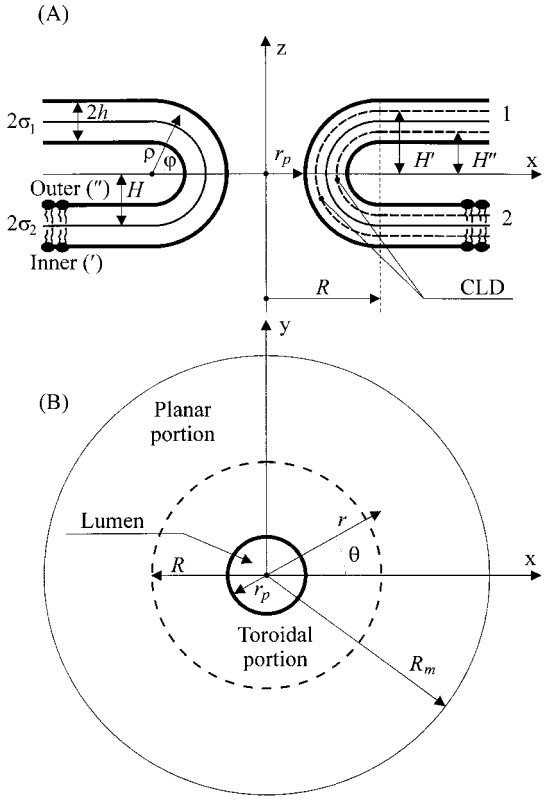

FIGURE 1 A toroidal fusion pore connecting two planar membranes, 1 and 2, at different tensions, $2\sigma_1$ and $2\sigma_2$, with $2\sigma_1 > 2\sigma_2$. (*A*) Cross-sectional side view of the system in x, z coordinates. The membrane-solution interfaces are represented by bold solid lines, and the surfaces of constant lipid density (CLD), for each monolayer, are shown as dashed lines. The interfaces between monolayers are denoted by the thin solid lines. (*B*) Top view of the system in x, y coordinates. The walls of the toroidal pore meet the planar membranes at radius R. The radius of the narrowest portion of the water-filled pore lumen is given by r_p. Thus the toroidal part of the membrane lies between r_p and R. The coordinate systems (x, y, z), (r, θ, z), and (ρ, φ, θ) illustrated here are described in the main text and Appendix A.

inner monolayer (the monolayer lining the pore lumen, Fig. 1), a greater area is available to a lipid headgroup than to the acyl chains (i.e., the distance ρ, Fig. 1, is greater in the headgroup region than for the acyl chains). As a consequence, the region occupied by the headgroups is expanded relative to the portion filled by the acyl chains, which is compressed. For the outer monolayer (the monolayer contacting the extracellular space), the opposite situation pertains. We avoid the mathematical complexities of treating a curved monolayer of finite thickness with nonconstant density by choosing within each monolayer a surface of constant lipid density (CLD) that lies between the polar headgroups and the hydrophobic acyl chains (Chizmadzhev et al., 1999). The lipid density within this surface is the same as that of the planar membranes. (The neutral surface, often used as a referent, is defined as the surface on which deformations of bending and area extension are independent of each other (Kozlov and Winterhalter, 1991). The surface of CLD and the neutral surface, defined differently, are not necessarily the same. But the pivotal plane (Leikin et al., 1996)—a surface where the area per lipid does not change with membrane deformations—is a surface of CLD.) In this way the fluid mechanical problem of lipid flow is reduced to a two-dimensional problem of flow of an incompressible liquid, with the two surfaces of the CLD interacting with each other through the relative viscosity. To allow explicit calculations, we assume that a surface of CLD is located in the middle of its monolayer (i.e., at $\rho = H \pm h/2$).

THEORY

Velocity distributions

We will consider separately the lipid velocities in the upper planar membrane (Fig. 1 *A*, 1), the lower planar membrane (Fig. 1 *A*, 2), and the toroidal surface of the pore. We will then match the velocities at the junctions of the toroidal pore with both planar membranes ($r = R$). For definiteness, we choose the positive direction of velocity as motion away from the z axis for membrane 1 and toward the z axis for membrane 2. In other words, velocity is positive for flow from membrane 2 to membrane 1. By reason of symmetry, lipid flow is radial in the planar portions of the membranes.

From conservation of area for any element of the membrane, lipid velocity is

$$\upsilon_r^{\prime,\prime\prime}(r) = \begin{cases} \upsilon_1^{\prime,\prime\prime}\dfrac{R}{r} & \text{for membrane 1 (upper membrane)} \\ \upsilon_2^{\prime,\prime\prime}\dfrac{R}{r} & \text{for membrane 2 (lower membrane)} \end{cases} \tag{1}$$

where $\upsilon_r^{\prime}$ and $\upsilon_r^{\prime\prime}$ are the velocities in the two respective monolayers at r. $\upsilon_{1,2}^{\prime}$ and $\upsilon_{1,2}^{\prime\prime}$, which need to be determined, are the linear velocities of lipids in the two monolayers at $r = R$. The subscripts 1 and 2 correspond to membranes 1 and 2, and the superscripts $\prime$ and $\prime\prime$ denote the surfaces of CLD of the inner and outer monolayers, respectively. Double superscripts are used when the equations have the same form for both monolayers.

To obtain the lipid velocity on the toroidal portion of the pore, we again employ the principle that the area of any element of membrane is conserved as it moves through the pore. We temporarily drop the superscripts $\prime$ and $\prime\prime$ because expressions for lipid velocity are the same for each monolayer. For a pore to expand, for any portion of a toroidal surface of CLD enclosed between angles 0 and φ, a net influx of lipid from the planar membrane into the toroidal pore must occur because the area of the surface of CLD within the toroid increases. This is a redistribution of lipid between the planar and toroidal portions of the membranes and not a net flux of lipid from one planar membrane to the other. There is, however, a net flux of lipids between planar membranes through the pore, referred to as "transpore" flux, because of differences in membrane tensions. In other words, pore growth leads to an accumulation of lipid within the walls of the pore; transpore flux does not.

To calculate the lipid flow, we use a moving coordinate system that is fixed to and moves with the CLD surface. The area enclosed between angles 0 and φ is

$$S(\varphi) = 2\pi\int_0^{\varphi} H(R - H\cos\phi)\mathrm{d}\phi = 2\pi HR\varphi - 2\pi H^2\sin\varphi \tag{2}$$

Only R is time-dependent, yielding

$$\frac{\mathrm{d}S}{\mathrm{d}t} = 2\pi H\varphi\upsilon_R \tag{3}$$

where $\upsilon_R = \mathrm{d}R/\mathrm{d}t$ is the translational velocity of the pore (i.e., the pore velocity). Because the area of the toroidal portion of a pore increases when the pore expands (or decreases when it shrinks) and because there is transpore flux, lipid flows at the boundaries 0 and φ according to

$$\frac{\mathrm{d}S}{\mathrm{d}t} = u(0)\cdot 2\pi r(0) - u(\varphi)\cdot 2\pi r(\varphi), \quad r(\varphi) = R - H\cos\varphi \tag{4}$$

where u is the lipid velocity in the moving coordinate system (e.g., $u(0)$ is the lipid velocity at the equatorial circumference, $\varphi = 0$). Because the velocity at the junction between the planar and toroidal portions of the membrane is to be determined (Eq. 1), it proves convenient to introduce the parameter υ as

$$u(0)\cdot 2\pi(R - H) = \upsilon\cdot 2\pi R \tag{5}$$

From Eqs. 3–5 we obtain for lipid velocity u

$$u(\varphi) = \frac{\upsilon R}{R - H\cos\varphi} - \frac{H\varphi\upsilon_R}{R - H\cos\varphi} \tag{6}$$

Ultimately we require the velocity of an element of membrane in the fixed coordinate system. This is obtained by adding $\upsilon_R \sin\varphi$ to Eq. 6 ($\upsilon_R \sin\varphi$ is the projection of pore velocity (υ_R is parallel to the planar membranes) onto the tangent of the CLD surface at any given φ). Reintroducing the superscripts $'$ and $''$ for inner and outer monolayers, we obtain

$$\upsilon'^{,''}_{\varphi} = \frac{\upsilon'^{,''}R}{R - H'^{,''}\cos\varphi} + \upsilon_R \sin\varphi - \frac{H'^{,''}\varphi\upsilon_R}{R - H'^{,''}\cos\varphi} \qquad (7)$$

where $H'^{,''}$ are the distances between surfaces of CLDs of corresponding monolayers (Fig. 1). By matching the lipid velocities (Eqs. 1 and 7) at the junction of the planar and toroidal portions ($r = R$ and $\varphi = \pm\pi/2$), we eliminate the unknown constants $\upsilon'^{,''}_{1,2}$ and obtain the velocity distribution in the planar portions as

$$\upsilon'^{,''}_{r} = \frac{R}{r}\left(\upsilon'^{,''} + \upsilon_R - \upsilon_R\frac{\pi H'^{,''}}{2R}\right) \quad \text{for membrane 1} \qquad (8)$$

$$\upsilon'^{,''}_{r} = \frac{R}{r}\left(\upsilon'^{,''} - \upsilon_R + \upsilon_R\frac{\pi H'^{,''}}{2R}\right) \quad \text{for membrane 2} \qquad (9)$$

The velocity distributions, Eqs. 7–9, depend on the three independent parameters υ', υ'', and υ_R, which will be determined below. It is worth noting the physical meaning of the three terms in these three equations. The first term of each of them is the lipid velocity of transpore lipid flow and is identical to that obtained for an immobile, fixed pore (Eq. 3 of Chizmadzhev et al., 1999). It is symmetrical relative to the equatorial plane and thus is the same for the two membranes. The second term is lipid velocity due to simple lateral movement of the pore wall (translation) caused by pore expansion. The third term is the velocity of lipid that redistributes between the planar membranes and the toroidal pore when the pore expands or contracts. It is independent of transpore flux and thus does not vanish even when transpore lipid flow is zero. The influx of lipid into the toroid occurs because of lipid redistribution; the velocity of lipid influx is small for $R \gg H$ but is greater than the second term of lipid velocity (velocity due to pore translation) at $R \approx H$ because $\pi H/2R > 1$. As a result, lipid velocity can even be negative at $r = R$ when an expanding pore is small. In contrast to the first term, the second and third are antisymmetrical relative to the equatorial plane and $\varphi = 0$. As will be seen, an appreciation of the symmetries is important for understanding lipid flow and pore movement.

Pore dynamics

We use Lagrange's equations with dissipation (Goldstein, 1950) to describe the viscous motion in the system. Because the velocities (and fluxes) quickly reach steady state, Lagrange's equations in our notation have the form

$$-\frac{\partial W}{\partial \xi_i} = \frac{\partial F}{\partial \dot{\xi}_i}, \quad W = W_b - W_\sigma \qquad (10)$$

where W is obtained from the bending energy of a curved pore wall, W_b, and the elastic energy, $-W_\sigma$, which is computed as the work done by the externally applied tensions $2\sigma_1$ and $2\sigma_2$. F is the dissipation function of the system that accounts for the frictional forces, and ξ_i are generalized coordinates describing the state of the system.

The choice of natural generalized coordinates becomes apparent by considering a single monolayer with total area A_m and external radii R_{m1} and R_{m2} in membranes 1 and 2, respectively. The work dW_σ done by tensions σ_1 and σ_2 to cause infinitesimal variations of R_{m1} and R_{m2}, with A_m remaining constant, is

$$dW_\sigma = \sigma_1 \cdot 2\pi R_{m1}\, dR_{m1} + \sigma_2 \cdot 2\pi R_{m2}\, dR_{m2} \qquad (11)$$

This equation can be rewritten as

$$dW_\sigma = \tfrac{1}{2}\sigma_+ d(\pi R_{m1}^2 + \pi R_{m2}^2) + \tfrac{1}{2}\sigma_- d(\pi R_{m1}^2 - \pi R_{m2}^2) \qquad (11')$$

where $\sigma_+ = \sigma_1 + \sigma_2$ and $\sigma_- = \sigma_1 - \sigma_2$.

The area A_m is given by

$$A_m = 2\pi H \cdot (\pi R - 2H) + \pi(R_{m1}^2 - R^2) + \pi(R_{m2}^2 - R^2) \qquad (12)$$

The first term in this expression is the area of the monolayer within the toroidal pore of radius R (Eq. 2), the second term is the area of the monolayer within the upper (1) planar membrane, and the third term is the area of the monolayer within the planar portion of the lower membrane (2). From Eq. 12 and $dA_m = 0$ and $dH = 0$ we obtain

$$\frac{1}{2} d(\pi R_{m1}^2 + \pi R_{m2}^2) = 2\pi\left(1 - \frac{\pi H}{2R}\right) R\, dR \qquad (12')$$

We introduce the variable A as

$$2A = \pi R_{m1}^2 - \pi R_{m2}^2 \qquad (13)$$

Substituting Eqs. 12′ and 13 into Eq. 11′, we obtain

$$dW_\sigma = \sigma_+ \cdot 2\pi R\left(1 - \frac{\pi H}{2R}\right) dR + \sigma_- \cdot dA \qquad (12'')$$

The right-hand side of Eq. 12″ is an exact differential, and, hence, W_σ is a state function (or a potential) of the system in the coordinates $\{A, R\}$. $\{A, R\}$ are natural generalized coordinates of the system: from Eq. 13 it is clear that the coordinate A describes lipid redistribution within the monolayer between membranes 1 and 2, while the coordinate R determines pore dynamics. The corresponding generalized velocities are $\dot{A}$, which provides transpore flux, and $\dot{R} = \upsilon_R$, which gives the velocity of the pore. $\dot{A}$ is related to

the lipid flow parameter v (Eqs. 7–9) by

$$\dot{A} = 2\pi R \cdot v \tag{14}$$

By reintroducing the superscripts $'$ and $''$ and remembering that the coordinate R is the same for the two monolayers, we obtain from Eq. 12″ that

$$dW_\sigma = \sigma_+ \cdot 4\pi R\left(1 - \frac{\pi H}{2R}\right)dR + \sigma_- \cdot dA_+ \tag{12‴}$$

where $A_+ = A' + A''$. It is useful to define a dual coordinate to A_+ as $A_- = A' - A''$. $\dot{A}_+$ and $\dot{A}_-$ are related to v' and v'' by expressions similar to Eq. 14:

$$\dot{A}_+ = 2\pi R \cdot v_+, \quad \dot{A}_- = 2\pi R \cdot v_- \tag{14′}$$

where $v_+ = v' + v''$ and $v_- = v' - v''$.

For reference, we use the fact that W_b depends only on R to rewrite Eq. 10 in coordinates $\{A_+, A_-, R\}$ as

$$\frac{\partial W_\sigma}{\partial A_+} = \frac{\partial F}{\partial \dot{A}_+}$$

$$\frac{\partial W_\sigma}{\partial A} = \frac{\partial F}{\partial \dot{A}} \tag{10′}$$

$$\frac{\partial W_\sigma}{\partial R} - \frac{\partial W_b}{\partial R} = \frac{\partial F}{\partial v_R}$$

We obtain directly explicit expressions for W_σ and the derivatives of W_σ on the left side of Eq. 10′ from Eq. 12‴ as

$$W_\sigma = 2\sigma_+ \pi R(R - \pi H) + \sigma_- A_+ + \text{const.}$$
$$\frac{\partial W_\sigma}{\partial R} = 4\pi R\left(1 - \frac{\pi H}{2R}\right), \quad \frac{\partial W_\sigma}{\partial A_+} = \sigma_-, \quad \frac{\partial W_\sigma}{\partial A_-} = 0 \tag{15}$$

We compute the derivative of W_b from the expression for bending energy of a membrane with zero spontaneous curvature (Helfrich, 1973), given as (Kozlov and Markin, 1983; Markin et al., 1984)

$$W_b(R) = 2\pi B \cdot \left(\frac{2R^2 \arctan\sqrt{\frac{R+H}{R-H}}}{H\sqrt{R^2 - H^2}} - 4\right) \tag{16}$$

where B is the membrane bending modulus.

To calculate the dissipation function, F, we use the relation (Goldstein, 1950)

$$F = \tfrac{1}{2}\dot{E} \tag{17}$$

and separate the dissipation rate $\dot{E}$ into two terms, one for dissipation due to shear (s) intramonolayer friction and the other due to relative (r) intermonolayer friction. That is,

$$\dot{E} = \dot{E}_s + \dot{E}_r \tag{18}$$

Shear dissipation for an incompressible fluid is calculated (Landau and Lifshitz, 1987) for each monolayer as

$$\dot{E}'_s = \frac{1}{2\eta_s}\int \sum_{j,k}(\sigma'_{jk})^2 dS' \tag{19}$$

where σ'_{jk} is the viscous stress tensor. Clearly, only radial and angular deformations are nonzero in the planar portions of the membranes. The corresponding elements of the viscous stress tensor are

$$\sigma'_{rr} = -\sigma'_{\theta\theta} = 2\eta_s \frac{v + v_R\left(1 - \frac{\pi H'}{2R}\right)}{r^2} R \tag{20}$$

In the toroidal portion, the only two nonzero components are given by (Appendix A)

$$\sigma'_{\varphi\varphi} = -\sigma'_{\theta\theta} = -2\eta_s\left[\frac{v' R \sin\varphi}{(R - H'\cos\varphi)^2} + \frac{v_R}{R - H'\cos\varphi} - \frac{v_R H' \varphi \sin\varphi}{(R - H'\cos\varphi)^2}\right] \tag{21}$$

The same expressions as Eqs. 20 and 21 hold for the outer monolayers, except that the index $'$ is replaced by $''$.

Substituting Eqs. 20 and 21 into Eq. 19 yields after integration

$$\dot{E}_s = \dot{E}^f_s(\dot{A}_+, \dot{A}_-, b) + 16\pi\eta_s M(b) \cdot v_R^2, \quad b = R/H \tag{22}$$

$$M(b) = \int_{-\pi/2}^{\pi/2} \frac{(b - \cos\varphi - \varphi\sin\varphi)^2}{(b - \cos\varphi)^3} d\varphi + \left(1 - \frac{\pi}{2b}\right)^2$$

where $\dot{E}^f_s$ is the dissipation rate of transpore lipid flow and does not depend on the rate of pore dilation or contraction. It can be shown that by using $\dot{A}_+$ and $\dot{A}_-$ as given by Eq. 14′, $\dot{E}^f_s$ is the same as the dissipation rate of lipid flow for a fixed pore (it is the sum of Eqs. B1 and B2 of Chizmadzhev et al., 1999). The second term in Eq. 22 provides the rate of energy dissipation due to pore movement.

The intermonolayer dissipation rate is (Evans and Hochmuth, 1978; Chizmadzhev et al., 1999)

$$\dot{E}_r = \frac{\eta_r}{h^2}\int (\Delta v)^2 dS \tag{23}$$

where

$$\Delta v = \begin{cases} v'_r - v''_r & \text{on planar membranes} \\ \left(\dfrac{v'_\varphi - v_R\sin\varphi}{H'} - \dfrac{v''_\varphi - v_R\sin\varphi}{H''}\right)H & \text{on toroidal wall} \end{cases} \tag{24}$$

Integration of Eq. 23 yields

$$\dot{E}_r = \dot{E}_r^f(\dot{A}_+, \dot{A}_-, b) + 16\pi\eta_r N(b)\cdot v_R^2$$
$$N(b) = \frac{1}{8}\int_{-\pi/2}^{\pi/2} \frac{\varphi^2\cos^2\varphi}{(b-\cos\varphi)^3}\,d\varphi + \frac{\pi^2}{16}\ln\frac{b_m}{b}, \quad b_m = \frac{R_m}{H} \tag{25}$$

where $\dot{E}_r^f$ is the rate of dissipation caused by lipid flow through a pore of fixed size (Chizmadzhev et al., 1999). As occurs for shear friction (Eq. 22 for $\dot{E}_s$), pore movement here additively contributes a term to relative friction (Eq. 25). Thus a most important conclusion has resulted from these calculations: the dissipation rates caused by both shear and relative friction separate into dissipation caused by transpore lipid flow (which is the same for an enlarging and a fixed size pore of the same size) and dissipation caused by pore growth. This separation is a consequence of the symmetry properties of the lipid velocity distributions (see discussion following Eq. 9).

We utilize this separation to rewrite the last equation of the system of Lagrange's equation (Eq. 10′), which depends on the variables v_R and R but not on A_+ and A_-, in the form

$$\frac{\partial W_\sigma}{\partial R} - \frac{\partial W_b}{\partial R} = \frac{\partial F_R}{\partial v_R} \tag{26}$$

where F_R is the portion of the dissipation function that depends only on v_R. From Eqs. 17, 22, and 25 we obtain

$$F_R = 8\pi v_R^2[\eta_s M(b) + \eta_r N(b)] \tag{27}$$

Using Eq. 15 for $\partial W_\sigma/\partial R$, Eq. 16 for W_b, and Eq. 27 for F_R, we obtain from Eq. 26 that the pore expansion velocity v_R is

$$v_R = \frac{dR}{dt} = \frac{-(dW_b/dR) + 2\pi R\sigma[1-(\pi H/2R)]}{16\pi[\eta_s M(R/H) + \eta_r N(R/H)]} \tag{28}$$

where $\sigma = 2\sigma_+ = 2(\sigma_1 + \sigma_2)$. Therefore, the rate of pore expansion depends only on the sum of the tensions (Eq. 28).

The velocity of the migration of the pore in radius space (i.e., the pore velocity) in response to a force is given by

$$v_R = -u_R\frac{d\tilde{W}(R)}{dR} \tag{29}$$

where $\tilde{W}$ is the potential of the force field, which governs pore movement. From Eq. 28, $\tilde{W}$ is given by

$$\tilde{W} = W_b - \tilde{W}_\sigma = W_b - \pi R^2\sigma + \pi^2 HR\sigma + \tilde{W}_0 \tag{30}$$

where $\tilde{W}_\sigma$ is obtained by integrating the second term of the numerator of Eq. 28 with respect to R, and $\tilde{W}_0$ is an integration constant that is independent of R. The pore mobility, u_R, is defined by the effective viscosity,

$$\tilde{\eta} = \eta_s M(b) + \eta_r N(b), \quad u_R = \frac{1}{16\pi\tilde{\eta}} \tag{31}$$

By comparing Eqs. 12‴ and 30, we see that $\tilde{W}(R)$ is the work necessary to form a pore of radius R at constant A_+ and A_-. Consequently, $\tilde{W}(R)$ is effectively the "partial free energy" of the pore and determines pore dynamics. We have thus rigorously shown that a toroidal fusion pore can be considered to be a quasiparticle that migrates in R-space with mobility u_R under the force field of $-d\tilde{W}(R)/dR$ and that both the mobility and force field can be explicitly calculated. Substituting Eqs. 30 and 31 into Eq. 29 yields the pore velocity, $v_R = dR/dt$, in the form

$$4\pi(4\tilde{\eta})\frac{dR}{dt} = 2\pi\sigma R - 2\pi\gamma(R) \tag{32}$$

where $\gamma(R)$ is the effective line tension of the fusion pore,

$$\gamma(R) = \frac{\pi}{2}H\sigma + \frac{1}{2\pi}\frac{dW_b}{dR} \tag{33}$$

Equation 32 is formally the same as the expression for the velocity of a pore within a single bilayer membrane with effective two-dimensional viscosity of $4\tilde{\eta}$ (Deryaguin and Gutop, 1962; Deryaguin and Prokhorov, 1981). The factor 4 appears because we assigned a two-dimensional viscosity to each monolayer and there is a total of four monolayers. Whereas line tension of a pore within a single bilayer is usually assumed to be independent of pore radius, in our treatment the line tension γ is explicitly calculated and is dependent on pore radius, R.

Because the bending energy, Eq. 16, is a nonlinear function of R, the differential equation (Eq. 28) must be solved numerically rather than analytically. In the case of a large pore, $R > 2H$, the bending energy W_b varies linearly with R and is given as

$$W_b = 2\pi\left(\frac{\pi B}{2H}\right)R + \text{const.} \tag{34}$$

Hence the line tension γ becomes independent of R:

$$\gamma = \frac{1}{2}\pi H\sigma + \frac{\pi B}{2H} \tag{35}$$

In this case Eq. 29 can be solved analytically as

$$R(t) = (R_0 - R_c)\exp\left(\frac{\sigma t}{8\tilde{\eta}}\right) + R_c, \quad R_c = \frac{\gamma}{\sigma} \tag{36}$$

where R_0 is the initial pore radius and R_c is a critical radius. For $R_0 > R_c$ the pore expands and for $R_0 < R_c$ the pore contracts. The characteristic time for pore evolution (expansion or contraction) is

$$\tau = \frac{8\tilde{\eta}}{\sigma} \tag{37}$$

Thus, for large pores, the radius increases exponentially with total tension, σ, as the driving force.

The lipid velocity distribution is defined by Eqs. 7–9, which contain the parameters v' and v'' (or, equivalently, v_+ and v_-) and v_R. v_R is given by Eq. 28. The variables v' and v'', which determine the transpore flux, are obtained from the first two Lagrange equations (Eq. 10′). Because neither v_+ nor v_- cross-multiplies with v_R, the first two Lagrange equations are independent of v_R (but dependent on $R(t)$). Therefore, the lipid velocities v' and v'' are independent of v_R and depend on the tension difference $2(\sigma_1 - \sigma_2)$, but not on the overall tension $2(\sigma_1 + \sigma_2)$. These lipid velocities are the same as those for a fixed pore as calculated previously (Chizmadzhev et al., 1999, Eqs. B2, B11, and B12). These equations for velocity provide a full and rigorous solution of lipid flow in the model. In conclusion, the tension gradient induces a transpore lipid flux, but it does not affect pore evolution; the sum of the tensions induces pore expansion but does not affect transpore lipid flux—that is, transpore lipid flux and pore expansion are independent of each other. Physically this occurs because lipids that move from one planar membrane to the other do not alter the number of lipids within the pore wall. Only the accumulation (or depletion) of lipids within the pore wall affects pore growth.

Pore dynamics is determined by the partial free energy, $\tilde{W}$, and mobility (Eqs. 28 and 31). We therefore examine the basic features of $\tilde{W}_\sigma$ and W_b, the two components of $\tilde{W}$, as a function of $r_p = R - H - h$. We illustrate the energies with the reasonable values $B = 10^{-12}$ erg (Niggemann et al., 1995), spontaneous membrane curvature, $K_s = 0$, $H = 10$ nm, and we pick $\sigma = 1$ dyn/cm for definiteness (Fig. 2). The work required to bend membranes into the toroidal shape of the pore wall varies with r_p. The bending energy, W_b, at first decreases steeply with increasing r_p, passes through a minimum, and then rises with a constant slope at $r_p > 10$ nm. W_b decreases for small r_p because the equatorial curvature decreases as r_p increases (i.e., the naturally flat, zero-spontaneous-curvature membrane has to bend less). Hence, if $\sigma = 0$, W_b does not reach a maximum. That is, the pore would not enlarge indefinitely without membrane tension, even though the pore wall could bend. Because dW_b/dr_p is much larger than $|d\tilde{W}_\sigma/dr_p|$, $\tilde{W}_\sigma$ does not greatly influence the shape of the curve of total energy $\tilde{W}(r_p)$ at $r_p < 10$ nm; $\tilde{W}_\sigma$ only causes a displacement of the entire $\tilde{W}$ curve along the energy axis for small r_p. Eventually the increases in area of the toroidal pore wall with r_p become the dominant effect on W_b, and thus W_b rises linearly with r_p (Eq. 34). But for r_p greater than ~10 nm, $-\tilde{W}_\sigma$ declines as r_p^2 (Eq. 31); the competition between the asymptotically increasing linear function of $W_b(r_p)$ and the decreasing parabolic function $\tilde{W}_\sigma(r_p)$ results in a maximum in $\tilde{W}(r_p)$ (Fig. 2, $\tilde{W}(r_p^{max}) = \tilde{W}_{max}$). The energy barrier between $\tilde{W}_{min}$ and $\tilde{W}_{max}$ is rather high (~$60kT$). For the toroidal pore the line tension depends on R and can be explicitly calculated from the total tension, $\sigma = 2(\sigma_1 + \sigma_2)$; the bending modulus of the membranes, B; and the separation of the membranes, H (Eq. 33). If $\sigma = 0$, $\tilde{W} = W_b$ and the energy of the toroidal pore keeps rising with increasing r_p (Fig. 2). In other words, the pore could never expand if $\sigma = 0$. The energy barrier is finite for $K_s = 0$ only if membrane tension is nonzero. As the tension becomes larger, the barrier height is lowered.

So far, it has been assumed that the spontaneous curvature $K_s = 0$. Increasing K_s from zero (Fig. 3, *curve 2*) to a positive value (*curve 1*) makes the slope of $W(r_p)$ steeper and the energy barrier becomes higher. Decreasing K_s to a negative value reduces the barrier, and if K_s becomes sufficiently negative, the barrier disappears completely (*curve 3*). In principle, fusion proteins could promote pore growth

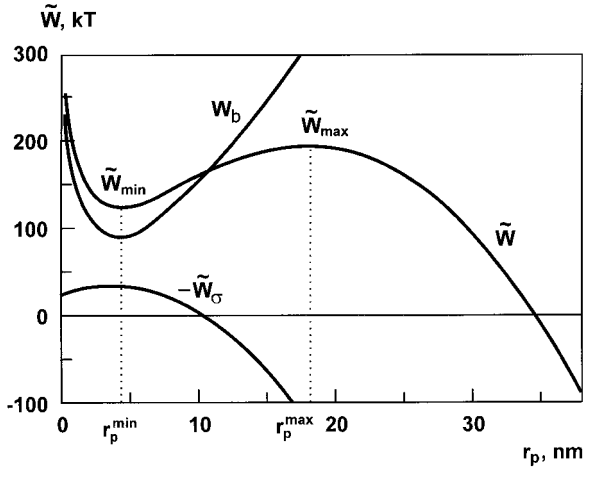

FIGURE 2 Toroidal pore partial free energy $\tilde{W} = W_b - \tilde{W}_\sigma$ and its components $-\tilde{W}_\sigma$ and W_b as functions of pore lumen radius $r_p = R - (H + h)$ for $h = 2$ nm, $H = 10$ nm, $B = 10^{-12}$ erg, $K_s = 0$, and $\sigma = 1$ dyn/cm.

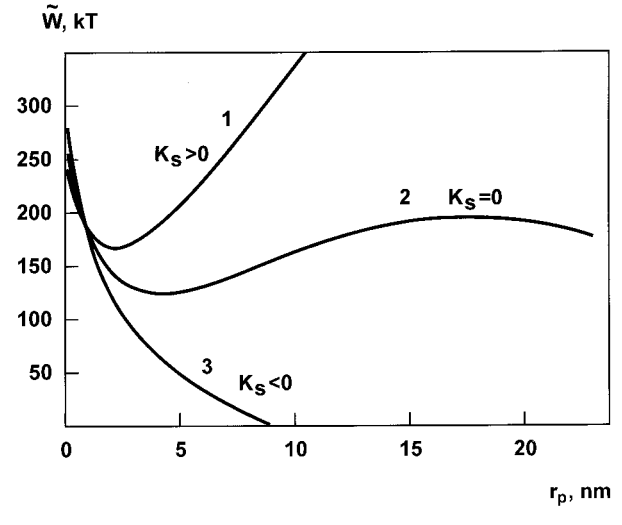

FIGURE 3 Toroidal pore partial free energy $\tilde{W}$ as a function of $r_p = R - (H + h)$ for different values of K_s. The values of K_s are 0.02 nm^{-1} (*curve 1*), 0 (*curve 2*), and -0.02 nm^{-1} (*curve 3*). Other values of the parameters are as in Fig. 3. The curves were calculated according to Eq. 31 and expressions for W_b given by Markin et al. (1984).

by effecting decreases in K_s. But K_s is determined by many molecular interactions and configurations such as local waters of hydration; we consider it unlikely that all fusion proteins could control pore growth, because it would be difficult to control a parameter that is affected by so many variables, each having its own regulating factors. To allow further consideration of how pore growth is controlled by membrane tension and pore length, we continue to use $K_s = 0$ in the remainder of this paper. (The displacement of all energy curves from zero is arbitrary, as is their placement with respect to each other. That is, the absolute values of energy shown in the graphs are not meaningful; only the shapes and therefore the differences in energy within each curve have numerical significance. This occurs because we choose the unfused state as the reference state to calculate energy differences, and this reference state varies with the conditions analyzed. As examples: in the unfused state, two parallel membranes under different tensions have different energies; the energies of unfused planar membranes change as K_s is varied.)

Whether a toroidal pore expands or contracts depends on its initial radius, r_p^0. If $0 < r_p^0 < r_p^{max}$ (where r_p^{max} is r_p of the energy barrier) the fusion pore will settle to $r_p = r_p^{min}$, while if $r_p > r_p^{max}$ the pore expands indefinitely, $r_p \to \infty$. Spontaneous contraction or expansion of an object, depending on whether it is smaller or larger than a critical size, is common to all theories of nucleation. For $r_p > r_p^{max}$ the line tension γ becomes independent of r_p (Eq. 35). If, because of thermal fluctuations, the barrier has been surmounted, r_p increases exponentially with a time constant given by Eq. 37, $\tau = 8\tilde{\eta}/\sigma$.

Growth of pores in a hemifusion diaphragm

Hemifusion, the merger of outer but not inner leaflets, is conjectured to be an intermediate of full fusion. At this intermediate, a single lipid bilayer, referred to as a hemifusion diaphragm, continues to separate aqueous phases. Lipid flows along the continuous outer monolayers because of the tension gradient. We consider the case in which the hemifusion diaphragm has extended somewhat to a radius R_d, but the diaphragm is still small compared to the size, R_m, of the fusing objects (Fig. 4, shown with a pore of radius R in the diaphragm). Because the two membranes are initially at different tensions, $2\sigma_1 > 2\sigma_2$, the two monolayers that comprise the hemifusion diaphragm are also under different tensions: the monolayer contributed by membrane 1 (monolayer (1)) is under tension $2\sigma_1$, and monolayer (2) is under tension $2\sigma_2$ (Fig. 4). We consider the pore while its radius is small compared to that of the diaphragm, $R \ll R_d$ (Fig. 4). The formation of this pore creates a continuous path for lipid flow from monolayer (2) to monolayer (1). We denote the velocities of lipids within monolayer (1) and (2) as v_1 and v_2, respectively (Fig. 4). We assume that lipid flow quickly becomes stationary and velocities are small. Characterizing the pore with a constant line tension γ (Deryaguin and Gutop, 1962; Deryaguin and Prokhorov, 1981) reduces the problem to a two-dimensional cylindrically symmetrical flow along two parallel planes. There is friction between the two flows. While flow rates can be determined by equating the work performed by tension with the dissipation due to friction (as was done above for the toroidal pore), it is more conveniently presented by locally balancing the tension gradient against intermonolayer friction as described by the Navier-Stokes equations,

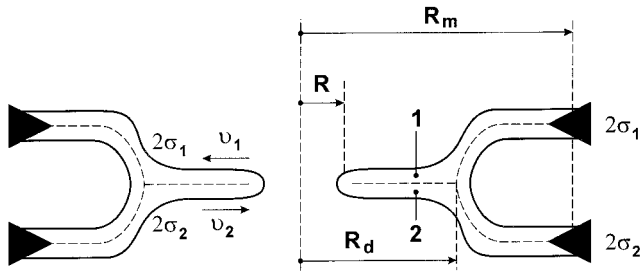

FIGURE 4 Schematic representation of a pore with radius R in a hemifusion diaphragm of radius R_d. The tensions of membranes 1 and 2 are given by $2\sigma_1$ and $2\sigma_2$. The tension at the border of the diaphragm must equal the sum of the tensions at the boundary of the system, $2\sigma_1 + 2\sigma_2$. The lipid velocity of each monolayer is given by v_1 and v_2. Monolayers 1 and 2 of the hemifusion diaphragm are indicated by numerals. The arrows designate the positive directions for lipid velocity within each monolayer.

$$\frac{d\sigma'}{dr} = \frac{\eta_r}{h^2}(v_1 + v_2) \tag{38}$$

$$\frac{d\sigma''}{dr} = -\frac{\eta_r}{h^2}(v_1 + v_2) \tag{39}$$

where $\sigma'(r)$ and $\sigma''(r)$ are the tensions at an arbitrary point r in monolayers (1) and (2). Obviously, the velocities v_1 and v_2 are not equal if the pore enlarges. Letting the tensions at the border of the diaphragm be equal to $2\sigma_1$ and $2\sigma_2$, the boundary conditions for Eq. (39) are

$$\sigma'(R_d) = 2\sigma_1, \quad \sigma''(R_d) = 2\sigma_2 \tag{40}$$

$$\sigma'(R) = \sigma''(R) \tag{41}$$

$$-2[\sigma'(R) + \sigma''(R)] + \frac{\gamma}{R} + \frac{2\eta_s}{R}[v_1(R) - v_2(R)] = 0 \tag{42}$$

Equation 42 is a balance of forces at the edge of the pore (Deryaguin and Gutop, 1962), with η_s describing the intramonolayer shear friction.

We introduce the variables

$$V = v_1(R) - v_2(R), \quad U = v_1(R) + v_2(R)$$
$$\sigma = 2(\sigma_1 + \sigma_2), \quad \Delta\sigma = 2(\sigma_1 - \sigma_2) \tag{43}$$

where V is twice the pore velocity dR/dt and U characterizes the rate of lipid exchange, through the pore, between mono-

layers. The lipid flux through the pore is equal to $2\pi R \cdot U$. The solution of Eqs. 38 and 39 in conjunction with the continuity equation, $\nabla \cdot \mathbf{v} = 0$, yields

$$\sigma'(R) = 2\sigma_1 - \frac{\eta_r}{h^2} U \ln \frac{R}{R_d},$$
$$\sigma''(R) = 2\sigma_2 + \frac{\eta_r}{h^2} U \ln \frac{R}{R_d} \quad (44)$$

From the boundary conditions, Eqs. 40–42, we obtain for V and U

$$V = \frac{\sigma}{2\eta_s}\left(R - \frac{\gamma}{\sigma}\right) \quad (45)$$

$$U = \frac{\Delta\sigma h^2}{2\eta_r R \ln \frac{R_d}{R}} \quad (46)$$

An inspection of Eqs. 45 and 46 shows that pore velocity, $V/2$, is limited by the intramonolayer shear viscosity, η_s, whereas the intermonolayer lipid flux $2\pi R \cdot U$ is controlled by the intermonolayer relative viscosity, η_r. It follows immediately from Eq. 45 that

$$\frac{dR}{dt} = \frac{\sigma}{4\eta_s}\left(R - \frac{\gamma}{\sigma}\right) \quad (47)$$

Equation 47 can be written in the form of Eq. 29, with $u_R = 1/8\pi\eta_s$ and partial free energy $\tilde{W}$ given by

$$\tilde{W} = -\pi R^2\sigma + 2\pi R\gamma \quad (48)$$

$\tilde{W}$ has a maximum at the critical radius, $R_c = \gamma/\sigma$. The partial free energy at the maximum of $\tilde{W}$ (compared to $R = 0$) is defined as the barrier height

$$\Delta\tilde{W}_{max} = \frac{\pi\gamma^2}{\sigma} \quad (48')$$

Differential Eq. 47 yields the solution

$$R(t) = (R_0 - R_c)\exp\left(\frac{\sigma}{4\eta_s} t\right) + R_c \quad (47')$$

where R_0 is the initial pore radius. Equation 47′ is similar to the time dependence of the radius of a large toroidal pore (Eq. 36). As is the case for a toroidal pore, a pore in a hemifusion diaphragm has as the driving force for enlargement the total tension $\sigma = 2(\sigma_1 + \sigma_2)$ (Eq. 45), while the tension difference $\Delta\sigma = 2(\sigma_1 - \sigma_2)$ drives the lipid flow between monolayers (Eq. 46).

DISCUSSION

The assumptions of the model

Biological fusion pores are not simply "holes" in hemifusion diaphragms, but rather are roughly toroidal in shape (Curran et al., 1993; Razinkov et al., 1998). We and others (Markin et al., 1984; Chernomordik et al., 1987; Nanavati et al., 1992; Siegel, 1993; Chizmadzhev et al., 1999) have modeled the pore as a mathematical toroid. The precise shape of a pore that minimizes the total energy, due to membrane bending and tension, can be obtained by the calculus of variations. Numerical solution of the resulting equations (written without accounting for lipid flow) shows that the exact shape is close to that of a toroid (Kumenko, Chizmadzhev, and Kuzmin, unpublished results). We have allowed the pore radius to vary but have maintained the intermembrane distance as a constant. To fuse vesicles and planar bilayers, for example, binding is induced by calcium. The calcium causes multiple sites of attachment and fixes intermembrane distances for long times (Niles et al., 1996). It is likely that these attachments remain after a fusion pore has formed, and thus we expect that pore length would remain constant. In biological fusion, pore length is probably controlled by the status of the fusion proteins, and thus we envision that the dynamics of pore length is controlled by protein rather than membrane mechanics. This means that the length of biological fusion pores can vary. We calculate the membrane mechanical energies of toroidal pores for different pore lengths and in this way consider the consequences of a nonconstant pore length (see below, Increasing pore length provides a convenient means of allowing enlargement of biological fusion pores).

We have assigned nonzero tensions to the fusing membranes because fusion pores are expected to be under tension. Planar bilayer membranes have significant tensions for a well-understood reason—the lipids are drawn into the supporting Gibbs-Plateau border. Vesicles also have membrane tensions whenever they swell, quantitatively accounted for by Laplace's relation. Vesicle swelling is routinely induced to fuse vesicles to planar membranes to reconstitute ion channels (Cohen and Niles, 1993), and in exocytosis, secretory granules often swell after a fusion pore forms (Zimmerberg et al., 1987; Breckenridge and Almers, 1987). In addition, measurements of lipid flux have shown that unswelled secretory granules (Monck et al., 1990) and intracellular granules (Sciaky et al., 1997) can also exhibit membrane tension; the physical reason for these tensions has not yet been elucidated. A fusion pore that forms between the plasma membranes of two cells will also be subject to membrane tension. The tension arises from interactions between the plasma membrane and cytoskeleton: the walls of a toroidal pore are dissociated from the cytoskeleton that normally adheres to a plasma membrane. The process of enlarging a pore thus requires that additional membrane be dissociated from the cytoskeleton. This is

analogous to pulling a tether out of a cell membrane, which also requires that the plasma membrane be dissociated from the cytoskeleton (Hochmuth et al., 1996; Dai and Sheetz, 1995; Waugh and Bauserman, 1995). If a force is not maintained on the tether, it withdraws back into the plasma membrane. The tension each cell exerts on the wall of a fusion pore should be approximately the same as the tension that pulls on the tether. Because the sum of the tensions affects pore growth, it is essential that membrane tension be incorporated into any theory that seeks to describe pore growth.

Fusion pore dynamics

We have described the evolution of pores with a physical approach that was developed to elucidate nucleation phenomena (Kramers, 1940; Zeldovich, 1942) and that has been profitably adapted to explain the metastability of thin films (Deryaguin and Gutop, 1962; Deryaguin and Prokhorov, 1981). In the case of nucleation, the size of the nucleus changes because of the flux of material (due to both diffusion and convection) onto and away from the nucleating interface. This is quantitatively described by a Fokker-Planck equation (Lifshitz and Pitaevskii, 1981; Kubo et al., 1991). When the nucleus reaches a critical size, it grows irreversibly. In a similar manner, a pore is treated as a "quasiparticle" that both diffuses and migrates in "radius space" in response to forces (Pastushenko et al., 1979). For a pore in a single bilayer, the force acting on the quasiparticle is calculated from the gradient of (Deryaguin and Gutop, 1962)

$$W = -\pi R^2\sigma + 2\pi R\gamma \qquad (49)$$

where W is the minimal work required to form a pore of radius R and γ is the line tension, independent of R. W has an energy barrier of $\pi\gamma^2/\sigma$ at the critical radius $R_c = \gamma/\sigma$. That is, when the pore is small ($R < R_c$), it spontaneously contracts. But if, because of thermal fluctuations, the pore does reach the critical radius, the radius migrates in the force field, $-dW/dR$, the pore expands indefinitely, and the membrane ruptures.

We have now demonstrated that a toroidal fusion pore can also be treated as a quasiparticle and have provided explicit equations (Eqs. 29–31) for the mobility of the quasiparticle and the forces acting upon it. We have further shown that the equations for the enlargement of a toroidal pore can be cast into the same form (Eq. 32) as those used to describe a pore in a single bilayer. The line tension of the pore in a single bilayer is replaced by an effective line tension that depends on the sum of the membrane tensions, the pore length ($2H$), and the variation of bending energy with pore radius (Eq. 33). Tensions of biological membranes can have profound effects on the ability of a fusion pore to enlarge, as we will discuss below. The tensions of fusing membranes will generally not be the same, and lipid will consequently flow from the low- to high-tension membrane. It might be thought that this flow could affect pore growth. But we have now rigorously shown that, in fact, the tension gradient does not affect pore dynamics. Pore expansion and transpore lipid flow are independent of each other. This conceptually useful result occurs mathematically because terms associated with pore expansion (R, v_R) and lipid flow (A_+, A_-) appear additively in the expressions for the energy (Eqs. 15 and 16) and the dissipation function (Eqs. 17, 22, 25) without cross-multiplication between them. As a direct consequence, Lagrange's equation (the third of Eq. 10′) for pore velocity separates from the other two Lagrange equations describing lipid flux. Pore expansion depends on the sum of the tensions, $2(\sigma_1 + \sigma_2)$; lipid flow depends on tension difference $2(\sigma_1 - \sigma_2)$ and is identical to that obtained for a pore of fixed radius (Chizmadzhev et al., 1999).

The theory can account for experimentally observed pore growth

Because the dynamics of pore growth is determined by the effective viscosity and membrane tension, we explicitly consider these terms. The effective viscosity $\tilde{\eta}$ (Eq. 30) depends on η_s, η_r, and the geometrical factors, $M(b)$ and $N(b)$ for shear and relative friction, respectively (Fig. 5, *bold curves*). Both the toroidal and planar portions of the membranes (Fig. 5, *thin curves*) contribute to these geometrical factors. The relative, intermonolayer friction is of much greater consequence in the planar portion than in the toroidal portion of the system, and $N(b)$ decreases with increasing R (Fig. 5 *A*). In contrast, if the pore is not too large ($R < 3H$), the toroidal portion of the system contributes most to the shear, intramonolayer friction (Fig. 5 *B*). $M(b)$ monotonically decreases with pore radius and approaches 1 asymptotically for a huge pore ($b \to \infty$). $N(b)$ also approaches a constant value asymptotically for a large pore: $N \approx 5$ for cell-cell fusion and $N \approx 8$ for fusion between significantly larger planar membranes (Fig. 5 *A*).

Measured values of shear and relative viscosities lie in the broad range of 10^{-7} g/s $< \eta_s < 10^{-3}$ g/s and 4×10^{-10} g/s $< \eta_r < 2 \times 10^{-4}$ g/s. (Evans and Hochmuth, 1978; Melikyan et al., 1985; Merkel et al., 1989; Evans et al., 1992; Evans and Young, 1994; Rafael and Waugh, 1996; Dai and Sheetz, 1995; Kumenko et al., 1999). For our subsequent discussion, we use for a model planar lipid bilayer membrane $\eta_s \approx \eta_r \approx 5 \times 10^{-6}$ g/s, and for a biological membrane we take $\eta_s \approx \eta_r \approx 5 \times 10^{-5}$ g/s, as discussed previously (Chizmadzhev et al., 1999).

Tensions of planar bilayer membranes lie in the range 0.2–4 dyn/cm (Tien, 1974; Chernomordik et al., 1987). Those of biological membranes are smaller. Tensions of plasma membranes that arise from interactions between lipids and proteins within the plane of the membrane are quite small, $\sim 10^{-2}$ dyn/cm if a cell is not osmotically

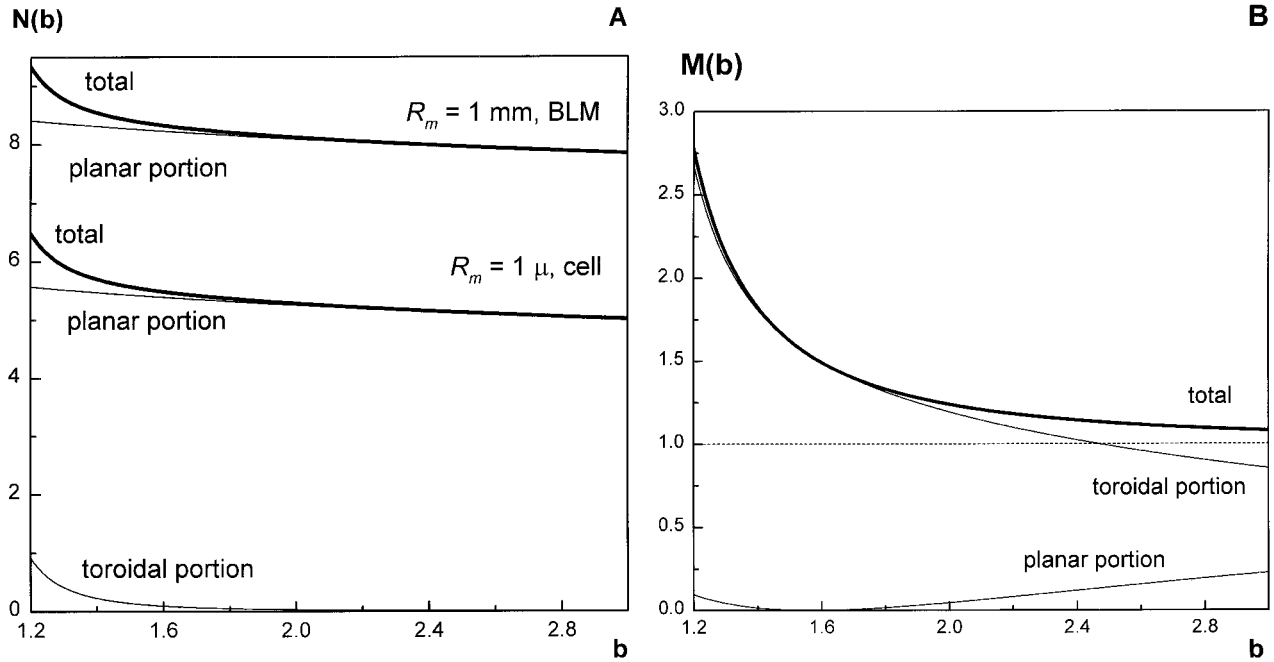

FIGURE 5 The dependence of the geometrical form factors $N(b)$ (A) and $M(b)$ (B) on the dimensionless pore radius $b = R/H$. The contributions of the toroidal and planar portions of the membranes to these form factors are as described in the text.

stressed (Dai and Sheetz, 1995). The tension arising from interactions between the membrane and cytoskeleton is usually significantly higher. In the case of red blood cells, for example, it is ~0.3 dyn/cm (Waugh and Bauserman, 1995). Fusion pores can remain at a small size for long times before they overcome the energy barrier. Once they do so, they rapidly enlarge with time constant τ. For enlargement of a pore in a lipid bilayer, we obtain from Eq. 47′ that $\tau \approx 5\ \mu$s for $\eta_s \approx 5 \times 10^{-6}$ g/s and total tension $\sigma \approx 1$ dyn/cm. This is in accord with the experimentally measured time constant for the exponential increase of pore conductance in planar membranes (Sukharev et al., 1983). Another example of how the present theory accounts for experimental observations is exocytotic fusion in mast cells. Lipid flux measurements indicate that the granules are under significant tension (Monck et al., 1990). From the measured lipid flux, the granules have been calculated to be under a tension of ~0.2 dyn/cm greater than that of the plasma membrane (Chizmadzhev et al., 1999). Assuming a viscosity of $\eta_s \approx 5 \times 10^{-5}$ g/s and a negligible plasma membrane tension, Eq. 37 yields $\tau \approx 30$ ms. This value is in the range (10–100 ms) of the observed time constants for full enlargement of fusion pores in mast cells (Curran et al., 1993). Another example is in cells expressing viral fusion proteins that have been fused to planar membranes. To calculate time constants, for the total tension we take $\sigma = 1$ dyn/cm, which is typical for planar bilayer membranes (Tien, 1974), and we use the viscosity of biological membranes because this membrane limits lipid movement more than the less viscous planar bilayer. The time constant for the increase in conductance upon full pore expansion is calculated from Eq. 37 to be $\tau = 3$ ms. This is in accord with the experimental observations (Melikyan et al., 1995, 1997). In short, the theory of the present study accounts for the rapid rise of conductance of final pore expansion. Furthermore, if these rise times can be measured, Eqs. 36 and 47 can be used to infer the membrane tensions and viscosities of the fusing membranes.

Lowering the energy barriers for fusion pores between vesicles and planar phospholipid bilayers

Vesicles are routinely fused, through osmotic swelling, to planar membranes to reconstitute channels incorporated in vesicle membranes into planar membranes (Cohen and Niles, 1993). Once formed, the fusion pores open fully, faster than can be experimentally measured (Cohen et al., 1980, 1984; Chernomordik et al., 1995; Chanturiya et al., 1997). For many lipid mixtures, hemifusion does not occur between vesicles and planar membranes in the absence of an osmotic gradient (Niles and Cohen, 1987; Niles et al., 1996). Upon application of the gradient fusion occurs, and the reason pores immediately enlarge can be readily appreciated: for $\sigma = 1$ dyn/cm, typical for planar membranes, a pore will reside in the potential well at r_p^{min} and have to overcome the high (~60kT) barrier (Fig. 6, *curve 1*). Swelling of vesicles increases the tension of their membranes and therefore increases the total tension, σ. Progressive in-

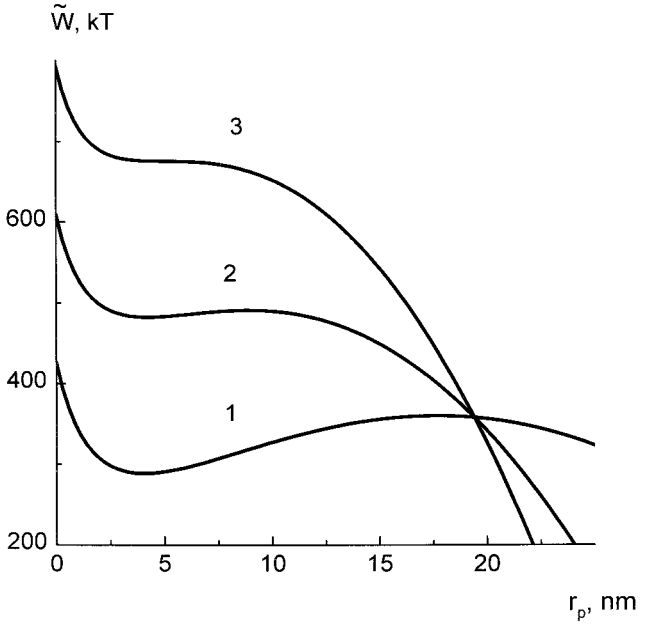

FIGURE 6 Toroidal pore partial free energy $\tilde{W}$ as a function of r_p for different total tensions. Numbers on the curves correspond to the value of σ in dyn/cm. All other parameters are the same as given in Fig. 2.

creases in σ decrease the barrier in $\tilde{W}(r_p)$. The barrier height decreases from $\sim 60kT$ for $\sigma = 1$ dyn/cm to $\sim 10kT$ for $\sigma = 2$ dyn/cm (*curve 2*), and for $\sigma = 3$ dyn/cm the barrier is eliminated (*curve 3*). Pore enlargement is rapid after a pore has grown beyond r_p^{max}.

For other lipid mixtures, hemifusion occurs between flaccid vesicles and planar membranes (Chernomordik et al., 1995). Pores form within an extended hemifusion diaphragm, but still do not enlarge unless the vesicles are osmotically swollen (Chanturiya et al., 1997). We illustrate concretely how increased vesicular tension promotes pore enlargement for a pore within the hemifusion diaphragm. Consider a hemifusion diaphragm comprising monolayers 1 and 2. The height of the barrier that prevents pore expansion varies as $\pi\gamma^2/2(\sigma_1 + \sigma_2)$ (Eq. 48′). We take the initial tension of the hemifusion diaphragm to be $\sigma_i = 1$ dyn/cm and let a pore within the diaphragm have a lifetime of τ_i. We estimate how much σ_i needs to be increased to greatly decrease (here, by nine orders of magnitude) this lifetime to τ_f:

$$\frac{\tau_i}{\tau_f} \approx \exp\left[\frac{\pi\gamma^2}{kT}\left(\frac{1}{\sigma_i} - \frac{1}{\sigma_f}\right)\right] \qquad (50)$$

For $\tau_i/\tau_f = 10^9$ and the typical value $\gamma = 10^{-6}$ dyn, from Eq. 50 we obtain $\sigma_f \approx 1.25$ dyn/cm. In other words, a rather small increase in membrane tension ($\sigma_f - \sigma_i = 0.25$ dyn/cm) drastically decreases the time (e.g., from 1000 s to 1 μs) it takes for a pore in a hemifusion diaphragm to enlarge. This enlargement causes the fusion pore to transition from a small pore in a hemifusion diaphragm (Fig. 7 *A*) to a toroidal pore that connects the two membranes (Fig. 7 *B*). We illustrate this sequence of events schematically (Fig. 7). For a pore in a hemifusion diaphragm, the increase in tension from σ_i to σ_f diminishes the height of the barrier and shifts its position, R_{max}, to smaller values (*solid curve* to *dotted curve*, Fig. 7 *A*). This allows the pore to enlarge to a toroidal shape with a radius equal to that of the hemifusion diaphragm, R_d (transition shown by *solid arrow* from Fig. 7

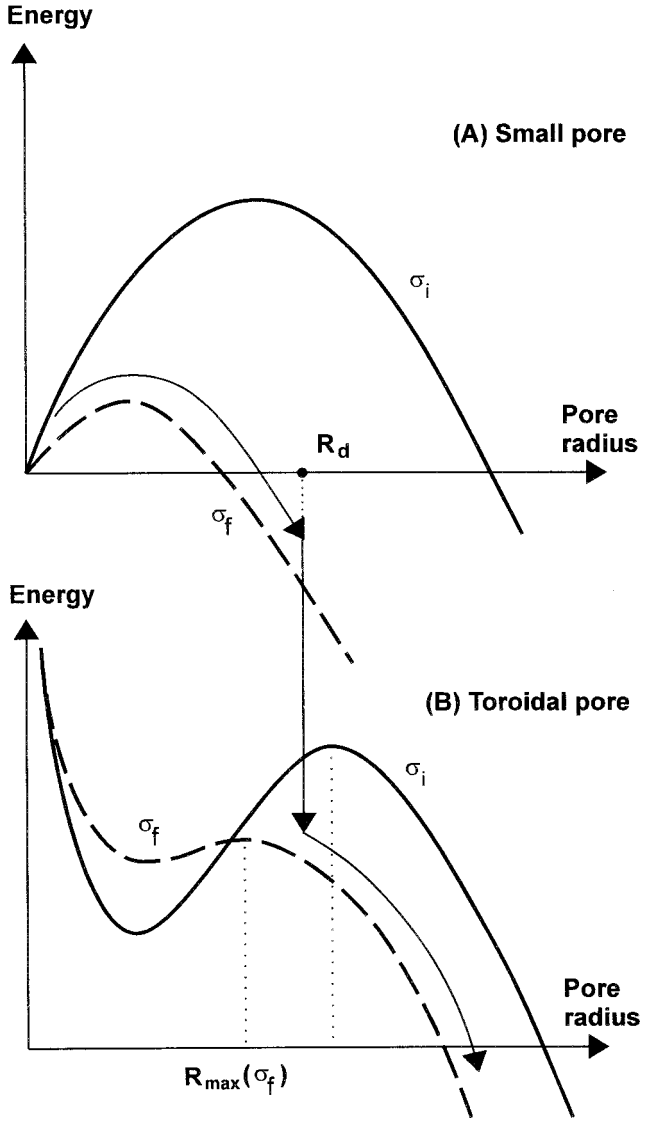

FIGURE 7 Schematic representation of the partial free energy of a small pore in a hemifusion diaphragm (*A*) and of a toroidal pore connecting two membranes (*B*). Solid curves correspond to the case of low overall initial tension σ_i; dotted curves give the energy after tension has been elevated to its final value, σ_f. The path shown by arrows within *A*, from *A* to *B*, and within *B* indicates the expansion of a small pore. The pore starts within a hemifusion diaphragm (of radius R_d), at less than its critical radius. With an increase in tension to σ_f, the pore radius easily becomes supercritical and the pore enlarges to the size of the diaphragm. At that point the pore has become toroidal (vertical transition from *A* to *B*) and further enlarges.

A to Fig. 7 *B*). Because σ has increased to σ_f, the barrier of the toroidal pore has already decreased and its R_{max} has been reduced (from *solid* to *dotted curve* in Fig. 7 *B*). If the radius of the toroidal pore (R_d) is greater than $R_{max}(\sigma_f)$, the pore continues to enlarge rapidly and fully.

Increasing pore length provides a convenient means of allowing enlargement of biological fusion pores

For biological membranes, tension will be less than $\sigma = 1$ dyn/cm, and the energy barrier will be even larger than the $60kT$ of Fig. 2. Pore growth is even less favorable under such conditions. The energetics set by membrane mechanics must be present, and yet pores enlarge significantly; in the case of virus, the pores enlarge so much that viral nucleocapsids, on the order of 100 nm in diameter, pass through and initiate infection. It is unlikely, in a biological situation, that changes in membrane tension and/or spontaneous curvature are utilized to lower the barrier; they are probably quite constant during pore growth. How, then, does a biological fusion pore overcome this large barrier? We propose that the barrier is lowered through increases in the length ($2H$, Fig. 1) of the toroidal pore.

Thus far in this paper we have fixed the length of the pore ($2H$). But as we have emphasized previously (Chizmadzhev et al., 1995), the length of a fusion pore can be a dynamic variable. A pore will widen if it can lengthen (Chizmadzhev et al., 1995), because the barrier against enlargement greatly decreases with increased pore length. We illustrate this for $\sigma = 0.6$ dyn/cm (Waugh and Bauserman, 1995). For $H =$ 10 nm, the energy barrier is large, $\sim 150kT$ (Fig. 8, *curve 1*); the pore is arrested within the potential well and it will not enlarge. However, the height of the barrier is only $35kT$ for $H = 15$ nm (*curve 2*) and has almost disappeared ($\sim 5kT$) at $H = 20$ nm (*curve 3*). If the sum of the tensions σ is smaller, for example, 0.3 dyn/cm, the barrier is $\sim 50kT$ at $H = 20$ nm (*curve 4*). For a very small total tension ($\sim$0.02 dyn/cm) the barrier can still disappear, but the pore must become very long, $H \approx 100$ nm. Freeze-fracture microscopy shows that in actuality, a pore does exhibit significant length when it has a large lumen (e.g., for figure 7 of Curran et al., 1993, the pore has an outside diameter of $\sim$20 nm, including the thickness of the membrane walls, and the pore length is $\sim$40 nm).

Fusion proteins locally decrease the distances between two membranes during the process that leads to pore formation. In the bound state, the membranes are separated by

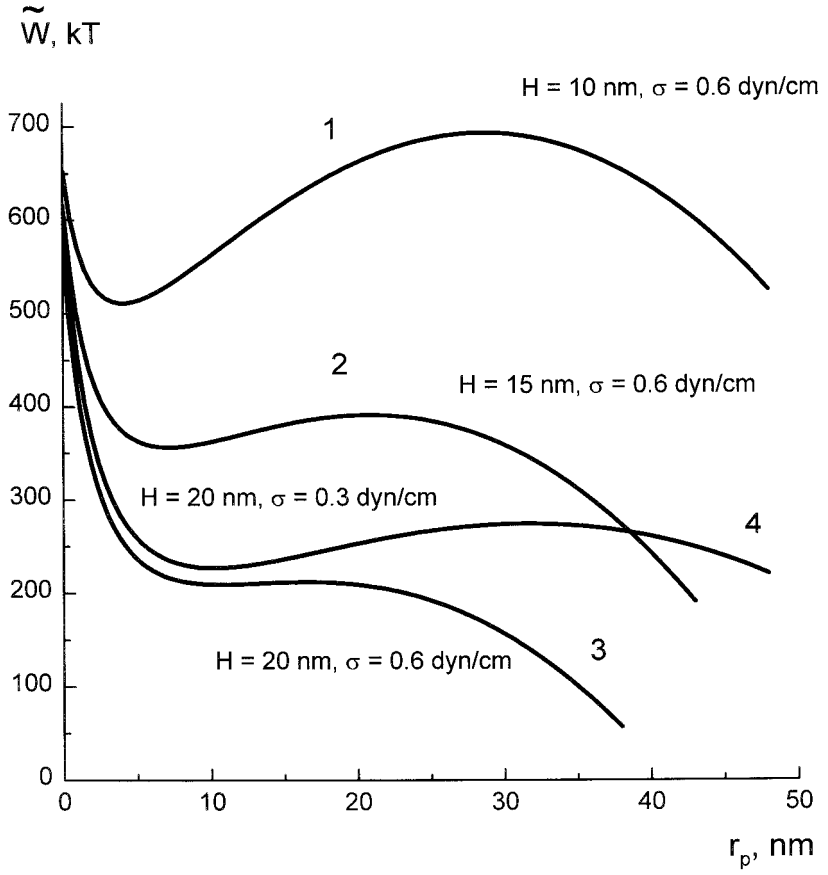

FIGURE 8 Toroidal pore partial free energy $\tilde{W}$ as a function of r_p for different values of H (*curves 1, 2, and 3*). The energy barrier is lower for large H. Lowering of σ from 0.6 to 0.3 dyn/cm (*curve 4*) leads to a larger energy barrier, but for $H = 20$ nm, the barrier is small, even for the lower tension.

the length of fusion proteins, on the order of 15 nm (Weissenhorn et al., 1999). For the membranes to come together, the proteins must undergo a series of conformational changes, thereby expending the energy stored in the proteins during folding (Trombetta and Helenius, 1998). At the point of pore formation, the proteins should be in a low-energy conformation, no longer forcing the membranes to remain close at the site of merger (for a review, see Hernandez et al., 1996). The fusion pore now resides in the energy well, which decreases for greater H (Fig. 8; for constant tension the reference energy of unfused membranes is constant and the displacement of curves 1, 2, and 3 with respect to each other is meaningful). The height of the barrier also decreases for greater H. The pore will naturally tend to minimize its energy and will therefore automatically lengthen while remaining in the canyon of the energy minimum. As it does so, it slowly widens (r_p^{min} increases for greater H; Fig. 8). The decrease in the energy barrier permits the pore to eventually fully expand (Chizmadzhev et al., 1995).

The lifetime of a pore in an energy well depends not only on the height of the barrier but also on the preexponential factor, K_0. K_0 may be estimated (e.g., see equations 7.16, 7.17, and 7.18 of Hänngi et al., 1990) as

$$K_0 \approx \frac{D_R}{L^2} \tag{51}$$

where L is the characteristic width of the potential well ($\sim$3 nm; Fig. 2) and D_R is the diffusion coefficient of the pore in R-space (R of Fig. 1). We estimate D_R from Eq. 31 (which gives pore mobility) and the relation between diffusion coefficients and mobility given by the Einstein equation

$$D_R = kT \cdot u_R = \frac{kT}{16\pi\tilde{\eta}} \tag{52}$$

Combining Eqs. 51 and 52 yields

$$K_0 \sim \frac{kT}{16\pi\tilde{\eta}L^2} \tag{53}$$

For $\tilde{\eta} \approx 10^{-4}$ g/s, we obtain $K_0 \approx 10^2$ s^{-1}.

As the pore lengthens, the energy barrier is reduced and the mean time needed to surmount the barrier is decreased. Thus the time between pore formation and full pore enlargement (pore lifetime) will be governed by the time of pore lengthening and the time it takes to surmount the energy barrier. For example, it would take $\sim$1 s to overcome a final barrier of $\sim 5kT$. For our chosen parameters, the pore would have to lengthen to $H = 20$ nm (Fig. 8, *curve 3*) to reduce the barrier to $5kT$. Thus, for a pore with a lifetime of several seconds, comparable times would be spent in pore lengthening and in surmounting the final barrier. For much longer-lived pores, the lifetime is probably determined by the rate at which the pore lengthens; for shorter-lived pores, pore lengthening would be rapid.

We envision that the time course for migration along the canyon of the energy minimum is determined in large part by the ease or difficulty with which membrane mechanics can force the fusion proteins to adjust their conformations to a lengthening pore. In other words, fusion is an active process on the part of the proteins until the point at which the pore is formed; then the membranes' mechanical energetics plays the active role as the pore enlarges.

The length a pore must achieve before the energy barrier is eliminated is sensitive to membrane tension. Our theoretical finding that the sum of tensions determines pore growth therefore takes on a potential biological importance. After formation of an exocytotic fusion pore, ion exchange between the granule lumen and extracellular space can cause decondensation of granule material with subsequent swelling of secretory granules (Zimmerberg et al., 1987; Curran and Brodwick, 1991; Curran et al., 1993; Parpura and Fernandez, 1996; Marszalek et al., 1997). Swelling could significantly increase the granule tension and thereby promote pore expansion—expansion that should accelerate the release of granule contents. Experimentally, pore dilation still occurs when granule swelling is osmotically prevented (Monck et al., 1991; Curran et al., 1993). But granule swelling does promote granule discharge (Chandler et al., 1989).

By deriving rigorous equations for the energies of toroidal pores as a function of membrane tension, we have been able to obtain a physically realistic framework for conceptualizing how biological fusion pores can enlarge. The biological process would not be obvious without quantitative exposition, but once the equations have been obtained, the importance of membrane mechanics in controlling the process of pore growth becomes apparent and logical.

APPENDIX A: THE COORDINATE SYSTEMS AND THE DIFFERENTIAL OPERATORS

So that this paper is self-contained, we provide the equations, used in our calculations, that depend on the chosen coordinate systems (exactly as given in Chizmadzhev et al., 1999). We use the cylindrical system of coordinates r, θ, z to calculate the velocity distribution in the planar portion of the system. They are related to Cartesian coordinates by the expressions (Fig. 1 *B*)

$$x = r\cos\theta \tag{A1}$$

$$y = r\sin\theta$$

$$z = z$$

Differential operators and the viscous stress tensor are transformed from Cartesian to curvilinear coordinates through the Lamé coefficients (Korn and Korn, 1968),

$$H_i = \sqrt{\left(\frac{\partial x}{\partial i}\right)^2 + \left(\frac{\partial y}{\partial i}\right)^2 + \left(\frac{\partial z}{\partial i}\right)^2} \tag{A2}$$

where $i = r, \theta, z$. Substituting Eq. A1 in Eq. A2 yields

$$H_r = 1, \quad H_\theta = r, \quad H_z = 1 \tag{A3}$$

An element of area is

$$dS = r\, d\theta\, dr \tag{A4}$$

The radial flow in the planar portions of the membranes depends on r only. The nonzero components of the viscous stress tensor can be written as

$$\sigma_{rr} = 2\eta \frac{\partial v_r}{\partial r}, \quad \sigma_{\theta\theta} = 2\eta \frac{v_r}{r} \tag{A5}$$

The system of coordinates ρ, φ, θ within the toroidal pore (Fig. 1) is related to Cartesian coordinates by

$$x = (R - \rho \cos \varphi)\cos \theta \tag{A6}$$

$$y = (R - \rho \cos \varphi)\sin \theta$$

$$z = \rho \sin \varphi$$

Substituting Eq. A6 into Eq. A2 for $i = \rho, \varphi, \theta$, we obtain

$$H_\rho = 1, \quad H_\varphi = \rho, \quad H_\theta = R - \rho \cos \varphi \tag{A7}$$

For an element of area we have

$$dS = \rho(R - \rho \cos \varphi)d\varphi\, d\theta \tag{A8}$$

A radius $r(\varphi)$ from the z axis of the pore to any point on the circumference of the toroidal surface is

$$r(\varphi) = R - \rho \cos \varphi \tag{A9}$$

The nonvanishing components of the viscous stress tensor have the form

$$\sigma_{\varphi\varphi} = 2\eta_s\left(\frac{1}{H_\varphi}\frac{\partial v_\varphi}{\partial \varphi} + \frac{v_\rho}{H_\rho H_\varphi}\frac{\partial H_\varphi}{\partial \rho}\right) \tag{A10}$$

$$\sigma_{\theta\theta} = 2\eta_s\left(\frac{v_\varphi}{H_\theta H_\varphi}\frac{\partial H_\theta}{\partial \varphi} + \frac{v_\rho}{H_\rho H_\theta}\frac{\partial H_\theta}{\partial \rho}\right) \tag{A11}$$

Substituting the velocity distributions; Eqs. 8 and 9, and H_φ, H_θ, H_ρ from Eq. A7, we obtain Eq. 21.

This work was supported in part by Fogarty International Research Collaboration Award R03 TW00715, National Institutes of Health grant GM 27367, the Russian Foundation for Basic Research (grants 94-04-50779, 96-15-97972, and 99-04-48426), and the Soros Educational Program.

REFERENCES

Breckenridge, L. J., and W. Almers. 1987. Final steps in exocytosis observed in a cell with giant secretory granules. *Proc. Natl. Acad. Sci. USA.* 84:1945–1949.

Chandler, D. E., M. Whitaker, and J. Zimmerberg. 1989. High molecular weight polymers block cortical granule exocytosis in sea urchin eggs at the level of granule matrix dissambly. *J. Cell. Biol.* 109:1269–1278.

Chanturiya, A., L. V. Chernomordik, and J. Zimmerberg. 1997. Flickering fusion pores comparable to initial exocytotic pores occur in protein-free phospholipid bilayers. *Proc. Natl. Acad. Sci. USA.* 94:14423–14428.

Chernomordik, L. V., A. Chanturiya, J. Green, and J. Zimmerberg. 1995. The hemifusion intermediate and its conversion to complete fusion: regulation by membrane composition. *Biophys. J.* 69:922–929.

Chernomordik, L. V., G. B. Melikyan, and Yu. A. Chizmadzhev. 1987. Biomembrane fusion: a new concept derived from studies using two interacting planar lipid bilayers. *Biochim. Biophys. Acta.* 906:309–352.

Chizmadzhev, Yu. A., F. S. Cohen, A. Shcherbakov, and J. Zimmerberg. 1995. Membrane mechanics can account for fusion pore dilation in stages. *Biophys. J.* 69:2489–2500.

Chizmadzhev, Yu. A., D. A. Kumenko, P. I. Kuzmin, J. Zimmerberg, and F. S. Cohen. 1999. Lipid flow through fusion pores connecting membranes of different tensions. *Biophys. J.* 76:2951–2965.

Cohen, F. S., M. H. Akabas, J. Zimmerberg, and A. Finkelstein. 1984. Parameters affecting the fusion of unilamellar phospholipid vesicles with planar bilayer membranes. *J. Cell Biol.* 98:1054–1062.

Cohen, F. S., and W. D. Niles. 1993. Reconstituting channels into planar membranes: a conceptual framework and optimal methods for fusion vesicles to planar bilayer phospholipid membranes. *Methods Enzymol.* 220:50–68.

Cohen, F. S., J. Zimmerberg, and A. Finkelstein. 1980. Fusion of phospholipid vesicles with planar phospholipid bilayer membranes. II. Incorporation of a vesicular membrane marker into the planar membrane. *J. Gen. Physiol.* 75:251–270.

Curran, M. J., and M. Brodwick. 1991. Ionic control of the size of the vesicle matrix of beige mouse mast cells. *J. Gen. Physiol.* 98:771–790.

Curran, M. J., F. S. Cohen, D. E. Chandler, P. J. Munson, and J. Zimmerberg. 1993. Exocytotic fusion pores exhibit semi-stable states. *J. Cell Biol.* 133:61–75.

Dai, J., and M. P. Sheetz. 1995. Regulation of endocytosis, exocytosis, and shape by membrane tension. *Cold Spring Harb. Symp. Quant. Biol.* 60:567–571.

Deryaguin, B. V., and Yu. V. Gutop. 1962. The theory of the rupture of free films. *Kolloidniy J.* 24:431–437 (in Russian).

Deryaguin, B. V., and A. V. Prokhorov. 1981. One the theory of the rupture of black films. *J. Colloid Interface Sci.* 81:108–115.

Evans, E. A., and R. M. Hochmuth. 1978. Mechanochemical properties of membranes. *Curr. Top. Membr. Transp.* 10:1–62.

Evans, E. A., and R. Skalak. 1980. Mechanics and Thermodynamics of Biomembranes. CRC Press, Boca Raton, FL. 1–254.

Evans, E. A., and A. A. Young. 1994. Hidden dynamics in rapid changes of bilayer shape. *Chem. Phys. Lipids.* 73:39–56.

Evans, E. A., A. Young, R. E. Waugh, and J. Song. 1992. Dynamic coupling and nonlocal curvature elasticity in bilayer membranes. *In* The Structure and Conformation of Amphiphilic Membranes. R. Lipowsky, D. Richter, and K. Kremer, editors. Springer-Verlag, Berlin. 148–153.

Goldstein, H. 1950. Classical Mechanics. Addison-Wesley, Reading, MA.

Hänggi, P., P. Talkner, and M. Borkovec. 1990. Reaction-rate theory: fifty years after Kramers. *Rev. Mod. Phys.* 62:251–341.

Helfrich, W. 1973. Elastic properties of lipid bilayers: theory and possible experiments. *Z. Naturforsch.* C28:693–703.

Hernandez, L. D., L. R. Hoffman, T. G. Wolfsberg, and J. M. White. 1996. Virus-cell and cell-cell fusion. *Annu. Rev. Cell. Dev. Biol.* 12:627–661.

Hochmuth, R. M., Jin-Yu Shao, J. Dai, and M. P. Sheetz. 1996. Deformation and flow of membrane into tethers extracted from neuronal growth cones. *Biophys. J.* 70:358–369.

Korn, G. A., and T. M. Korn. 1968. Mathematical Handbook, 2nd Ed. McGraw-Hill, New York.

Kozlov, M. M., and V. S. Markin. 1983. Possible mechanism of membrane fusion. *Biofisics.* 28:255–261.

Kozlov, M. M., and M. Winterhalter. 1991. Elastic moduli for strongly curved monolayers. Position of the neutral surface. *J. Phys. II France.* 1:1077–1084.

Kramers, H. A. 1940. Brownian motion in a field of force and the diffusion model of chemical reactions. *Physica.* 7:284–302.

Kubo, R., M. Toda, and N. Nashitsume. 1991. Statistical Physics II, 2nd Ed. Springer-Verlag, Berlin.

Kumenko, D. A., P. I. Kuzmin, and Yu. A. Chizmadzhev. 1999. Stalk dynamics and lipid flux in membrane hemifusion. *Biol. Membr.* 16: 472–480. (in Russian).

Landau, L. D., and E. M. Lifshitz. 1987. Fluid mechanics, 2nd Ed. Pergamon Press, Oxford.

Leikin, S., M. M. Kozlov, N. L. Fuller, and R. P. Rand. 1996. Measured effects of diacylglycerol on structural and elastic properties of phospholipid membranes. *Biophys. J.* 71:2623–2632.

Lifshitz, E. M., and L. P. Pitaevskii. 1981. Physical Kinetics. Pergamon Press, Oxford.

Markin, V. S., M. M. Kozlov, and V. L. Borovjagin. 1984. On the theory of membrane fusion. The stalk mechanism. *Gen. Physiol. Biophys.* 5:361–377.

Markosyan, R. M., G. B. Melikyan, and F. S. Cohen. 1999. Tension of membranes expressing the hemagglutinin of influenza virus inhibits fusion. *Biophys. J.* 77:943–952.

Marszalek, P. E., B. Farrell, P. Verdugo, and J. M. Fernandez. 1997. Kinetics of release of serotonin from isolated secretory granules. II. Ion exchange determines the diffusivity of serotonin. *Biophys. J.* 73: 1169–1183.

Melikyan, G. B., L. V. Chernomordik, and I. G. Abidor. 1985. Surface area expansion for trilaminar structure during monolayer membrane fusion. *Biol. Membr.* 2:1048–1054 (in Russian).

Melikyan, G. B., H. Jin, R. A. Lamb, and F. S. Cohen. 1997. The role of the cytoplasmic tail region of influenza virus hemagglutinin in formation and growth of fusion pores. *Virology.* 235:118–128.

Melikyan, G. B., W. D. Niles, and F. S. Cohen. 1995. The fusion kinetics of influenza hemagglutinin expressing cells to planar bilayer membranes is affected by HA density and host cell surface. *J. Gen. Physiol.* 106: 783–802.

Merkel, R., E. Sackmann, and E. A. Evans. 1989. Molecular friction and epitatic coupling between monolayers in supported bilayers. *J. Phys. France.* 50:1535–1555.

Monck, J. R., G. Alvarez de Toledo, and J. M. Fernandez. 1990. Tension in secretory granule membranes causes extensive membrane transfer through the exocytotic fusion pore. *Proc. Natl. Acad. Sci. USA.* 87: 7804–7808.

Monck, J. R., A. Oberhauser, G. Alvarez deToledo, and J. M. Fernandez. 1991. Is swelling of the secretory granule matrix the force that dilates the exocytotic fusion pore? *Biophys. J.* 59:39–47.

Nanavati, C., V. S. Markin, A. F. Oberhauser, and J. M. Fernandez. 1992. The exocytotic fusion pore modeled as a lipidic pore. *Biophys. J.* 63:1118–1132.

Niggemann, G., M. Kummrow, and W. Helfrich. 1995. The bending rigidity of phosphatidylcholine bilayers: dependences on experimental method, sample cell sealing and temperature. *J. Phys. France.* 5:413–425.

Niles, W. D., and F. S. Cohen. 1987. Video fluorescence microscopy studies of phospholipid vesicle fusion with a planar phospholipid membranes. Nature of membrane-membrane interactions and detection of contents release. *J. Gen. Physiol.* 90:703–735.

Niles, W. D., J. R. Silvius, and F. S. Cohen. 1996. Resonance energy transfer imaging of phospholipid vesicle interaction with a planar phospholipid membrane. *J. Gen. Physiol.* 107:329–351.

Parpura, V., and J. M. Fernandez. 1996. Atomic force microscopy study of the secretory granule lumen. *Biophys. J.* 71:2356–2366.

Pastushenko, V. F., Yu. A. Chizmadzhev, and V. B. Arakelyan. 1979. Calculation of the membrane life-time in the steady-state diffusion approximation. *Bioelectrochem. Bioenerget.* 6:53–62.

Raphael, R. M., and R. E. Waugh. 1996. Accelerated interleaflet transport of phosphatidylcholine molecules in membranes under deformation. *Biophys. J.* 71:1374–1388.

Razinkov, V. I., G. B. Melikyan, R. M. Epand, R. F. Epand, and F. S. Cohen. 1998. Effects of spontaneous bilayer curvature on influenza virus-mediated fusion pores. *J. Gen. Physiol.* 112:409–422.

Sciaky, N., J. Presley, C. Smith, K. J. Zaal, N. Cole, J. E. Moreira, M. Terasaki, E. Siggia, and J. Lippincott-Schwartz. 1997. Golgi tubule traffic and the effects of brefeldin A visualized in living cells. *J. Cell Biol.* 139:1137–1155.

Siegel, D. P. 1993. Energetics of intermediates in membrane fusion: comparision of stalk and inverted micellar intermediate mechanisms. *Biophys. J.* 65:2124–2140.

Solsona, C., B. Innicenti, and J. M. Fernandez. 1998. Regulation of exocytotic fusion by cell inflation. *Biophys. J.* 74:1061–1073.

Sukharev, S. I., V. B. Arakelyan, I. G. Abidor, L. V. Chernomordik, and V. F. Pastushenko. 1983. Rupture of planar BLM under influence of electric field. *Biophysica.* 28:756–760 (in Russian).

Tien, H. Ti. 1974. Bilayer Lipid Membranes (BLM): Theory and Practice. Marcel Dekker, New York.

Trombetta, E. S., and A. Helenius. 1998. Lectins as chaperones in glycoprotein folding. *Curr. Opin. Struct. Biol.* 8:587–592.

Waugh, R. E., and R. G. Bauserman. 1995. Physical measurements of bilayer-skeletal separation forces. *Ann. Biomed. Eng.* 23:308–321.

Weissenhorn, W., A. Dessen, L. J. Calder, S. C. Harrison, J. J. Skehel, and D. C. Wiley. 1999. Structural basis for membrane fusion by enveloped viruses. *Mol. Membr. Biol.* 16:3–9.

Zeldovich, Ja. B. 1942. Theory of cavitation in liquids. *Zhurnal Eksperim. Theor. Phys.* 12:525–532.

Zimmerberg, J., F. S. Cohen, and A. Finkelstein. 1980. Fusion of phospholipid vesicles with planar phospholipid bilayer membranes. I. Discharge of vesicular contents across the planar membrane. *J. Gen. Physiol.* 75:241–250.

Zimmerberg, J., M. Curran, F. S. Cohen, and M. Brodwick. 1987. Simultaneous electrical and optical measurements show that membrane fusion precedes secretory granule swelling during exocytosis of beige mouse mast cells. *Proc. Natl. Acad. Sci. USA.* 84:1585–1589.